Available online at www.sciencedirect.com
SCIENCE DIRECT
Polymer 47 (2006) 3528–3539
polymer
www.elsevier.com/locate/polymer

# TPO based nanocomposites. Part 2. Thermal expansion behavior

Hyuk-soo Lee [a], Paula D. Fasulo [b], William R. Rodgers [b], D.R. Paul [a,*]

[a] Department of Chemical Engineering and Texas Materials Institute, The University of Texas at Austin, Austin, TX 78712, USA
[b] General Motors Research and Development Center, 30500 Mound Road, Warren, MI 48090, USA

Received 19 January 2006; received in revised form 4 March 2006; accepted 6 March 2006
Available online 31 March 2006

**Abstract**

The linear thermal expansion behavior of thermoplastic polyolefin, or TPO, nanocomposites based on a polypropylene/elastomer/masterbatch mixture was examined using a thermomechanical analyzer (TMA). For these experiments the masterbatch consisted of a mixture of organoclay and maleated polypropylene. The nanocomposites were prepared in a twin-screw extruder. The effects of both the elastomer domains and the filler particles on the thermal expansion behavior of the nanocomposites were investigated by means of transmission electron microscopy (TEM) and atomic force microscopy (AFM). The addition of elastomer tends to increase the linear coefficient of thermal expansion, CTE. On the other hand, the addition of clay significantly reduces the thermal expansion in both the flow (FD) and transverse directions (TD) of injection molded specimens; however, the extent of reduction of CTE in the FD is much greater than in the TD. The CTE in the normal direction (ND) increases when either the clay or elastomer content is increased. The trends in thermal expansion for the nanocomposites are discussed in terms of the morphology of both dispersed clay and elastomer phases based on TEM and AFM observations and subsequent particle analyses.


*Keywords:* Polymer nanocomposites; Thermal expansion; TPO

## 1. Introduction

The high coefficient of thermal expansion, or CTE, of polymers has been a continuing concern as these lighter weight materials replace metals (low thermal expansion) as structural parts particularly in automotive applications [1,2]. The resulting mismatch in thermal expansion behavior can lead to problems in paint ovens or in use where, in principle, the external temperature may vary from −30 to +40 °C or more. The addition of fillers or reinforcing agents into plastics mitigates to some degree the high thermal expansion of these materials by two different mechanisms: (a) volume dilution with a material of lower CTE and (b) mechanical constraint by a dispersed phase with low CTE and high modulus. The latter is by far the more important effect for high aspect ratio fillers [1–5]. Indeed, glass fiber reinforcement can be an effective way of reducing the linear CTE of plastics [1,6]; however, because of the near macroscopic size of such fibers, the surface finish of such composites may be severely compromised. Polymer nanocomposites made by exfoliating the 1 nm thick aluminosilicate platelets of the clay-mineral montmorillonite (MMT) offer exciting possibilities for resolving these problems. These platelets possess a high modulus and high aspect ratios for effective reinforcement and mechanical restraint of thermal expansion, yet the particles are much too small to deteriorate surface finish [7]. The data in Fig. 1 shows that the addition of 7 wt% MMT into a 'thermoplastic polyolefin', or TPO, gives a comparable extent of reduction in thermal expansion as 25 wt% talc. The materials used in these experiments were prepared from commercial TPO formulations [8].

The first paper in this series described the mechanical properties and morphology of the type of nanocomposites mentioned above [9]. The purpose of this paper is to examine the morphology and thermal expansion behavior of the same polypropylene, or PP, materials reinforced with an organoclay and toughened with an ethylene–octene based elastomer (EOR) made by melt processing. An in-depth particle analysis for both filler and elastomer morphology along the flow and transverse directions for injection molded specimens is used to evaluate how both phases influence thermal expansion behavior of the nanocomposites. As expected, the thermal expansion characteristics of injection molded specimens depend strongly on the morphology of the dispersed clay and elastomer particles. In practical terms, the coefficient of thermal expansion is a major component of the post injection molding shrinkage of

* Corresponding author. Tel.: +1 512 471 5392; fax: +1 512 471 0542.
*E-mail address:* drp@che.utexas.edu (D.R. Paul).

0032-3861/$ - see front matter © 2006 Elsevier Ltd. All rights reserved.
doi:10.1016/j.polymer.2006.03.016

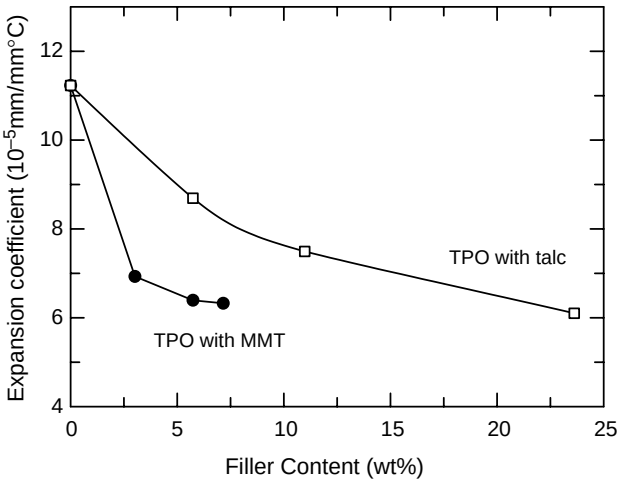


Fig. 1. Comparison of relative thermal expansion coefficient as a function of filler content of TPO composites formed from melt mixing with MMT and with talc; materials provided from [8].

a material. Therefore, a better understanding of the influence of the composite morphology on the coefficient of thermal expansion will lead to improved dimensional stability of injection molded parts.

## 2. Experimental

### 2.1. Materials and composite preparation

Nanocomposites were produced by melt compounding mixtures of PP (melt index = 37), an ethylene–octene based elastomer (melt index = 0.5), and a masterbatch material containing equal parts of maleated PP (PP-*g*-MA, MA content = 1.0 wt%) and an organically modified montmorillonite (di-methyl, dihydrogenated tallow montmorillonite). Extruded nanocomposites pellets were dried and then injection molded into standard tensile (ASTM D638, type I) and Izod (ASTM D256) specimens. Further details of the melt processing steps used to form and shape these materials are given in the first paper in this series [9].

### 2.2. Morphology characterization and particle analysis for the filler and elastomer

Samples for transmission electron microscopy (TEM) analysis were taken from the central region of an Izod bar. Sections taken from the core region of injection molded specimens were viewed parallel to the three orthogonal axes, flow direction (FD), transverse direction (TD) and normal direction (ND) (see Ref. [9] for schematic definition of these terms). TEM micrographs were taken on views observed parallel to the flow direction, or FD (TD–ND plane), and the transverse direction, or TD (FD–ND plane). The morphology viewed parallel to the normal direction, or ND, will be presented in a subsequent paper. This nomenclature is used throughout the remainder of this paper. The detailed geometry of the specimen and the viewing directions for TEM are given in the previous paper [9]. Ultra-thin sections ranging from 50 to 70 nm in thickness were cryogenically cut with a diamond knife at −65 °C for the specimen and −58 °C for the knife using a RMC PowerTome XL ultramicrotome. Sections were collected on 300 mesh copper TEM grids and subsequently dried with filter paper. The sections were examined using a JEOL 2010F TEM with a $LaB_6$ filament operating at an accelerating voltage of 120 kV. Complete details of the microtomy, microscopy, and image analysis techniques employed here are given in the previous paper [9].

Atomic force microscopy (AFM) experiments were performed at room temperature on cryogenically microtomed surfaces of nanocomposites containing elastomer using a Digital Instruments Dimension 3100 with Nanoscope IV controller. Images were recorded in the tapping mode using etched silicon probes. The instrumental parameters, such as the set point and gains, were adjusted to improve the image resolution. The particle analysis for the elastomer phase obtained by AFM images was done using a similar procedure as that used for TEM image analyses described in the previous paper [9].

### 2.3. Thermal expansion measurement

Thermal expansion tests were conducted according to ASTM D696 using a Perkin–Elmer thermomechanical analyzer (TMA 7). Rectangular specimens were prepared from the central region of Izod bars. The dimensions of the specimens were as follows: thickness = 3.2 mm, width = 6.4 mm, and height = 12.7 mm. Thermal expansion measurements were made in all three orthogonal directions, i.e. flow (FD), transverse (TD), and normal (ND) directions. Due to the thickness of the injection molded specimens, measurements made in the ND were performed on a stack of three specimens that were glued together using an instant adhesive. Each specimen was held at −40 °C for 5 min, followed by heating at a rate of 5 °C/min to 125 °C and subsequently held for 30 min, then quenched to room temperature. In order to assess both reversible and non-reversible effects, each specimen was stored at room temperature for at least 24 h after the first heating and then re-heated at a rate of 5 °C/min to 125 °C. All measurements were done in a nitrogen atmosphere.

## 3. Results and discussion

### 3.1. Morphology characterization using TEM and AFM

As addressed in the previous paper [9], the aspect ratio of MMT, i.e. particle length/particle thickness, is one of the important factors in determining the reinforcement efficiency of clay nanocomposites; however, a few studies have indicated that the shape of the MMT particle may be anisotropic, i.e. different lengths along the FD and TD. This observation was based on the morphology and thermal expansion behavior of nylon 6 nanocomposites [2,10,11]. Fig. 2 shows TEM micrographs of PP/masterbatch nanocomposites containing 6.8 wt% of MMT viewed parallel to the TD and FD. As shown for nylon 6 nanocomposites in this laboratory [2], there can be

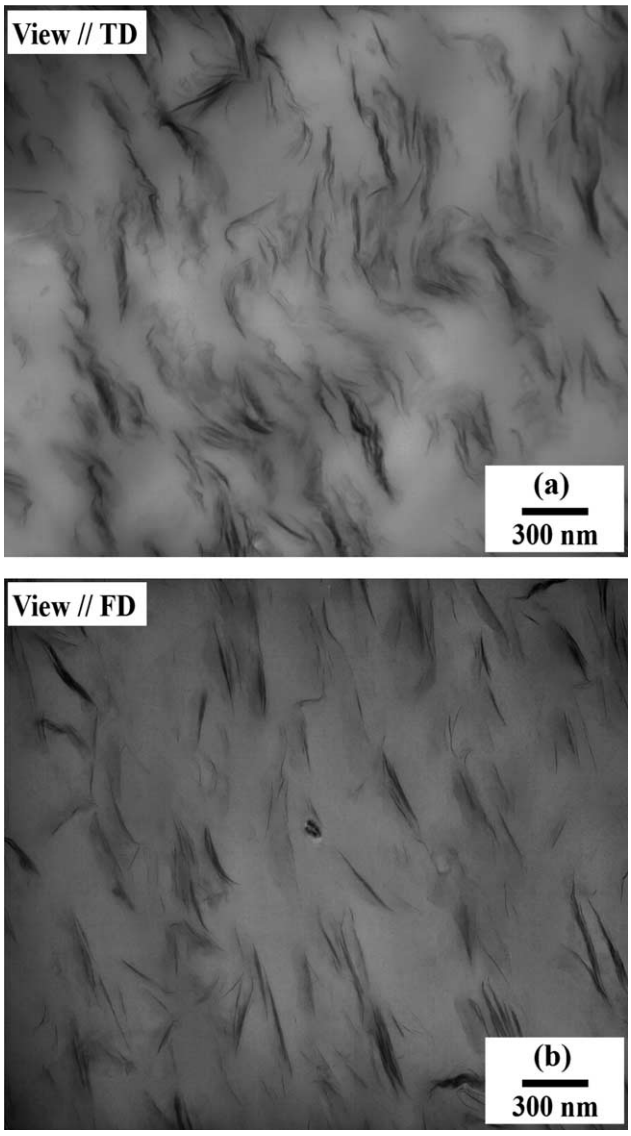


Fig. 2. TEM micrographs of PP/masterbatch nanocomposites containing 6.8 wt% MMT: sections (a) viewed parallel to the TD and (b) viewed parallel to the FD were taken from the core of injection molded specimens.

differences in orientation and length of clay particles along the FD and TD. Particles pointing in the flow direction seem longer and better aligned than those pointing in the transverse direction for these nylon 6 systems. However, for the current nanocomposites, opposite trends were observed in terms of shape and alignment of clay particles along the FD and TD The number of particles with a skewed and/or tilted shape in views parallel to the FD (TD–ND plane), Fig. 2(b), is significantly less than that observed in views parallel to the TD (FD–ND plane), Fig. 2(a); i.e. the particles seem to be better aligned along the TD than the FD. It also appears that more single platelets are visible in the view of TD–ND plane than in the view of FD–ND plane. Possible explanations for the discrepancies in the apparent dispersion of clay particles for the current nanocomposites, depending on the direction of observation, and the contrast with those based on nylon 6 will be discussed in more detail later.

As shown in the previous paper, the thickness of clay particles measured in views parallel to the TD increases with increasing MMT content in nanocomposites made from the PP/masterbatch. However, an opposite trend for particle thickness is observed from the views parallel to the FD, i.e. a decrease in particle thickness is observed with increasing MMT content. This may stem from the edges of the clay particles that were peeled apart by the shear stress during melt processing [12,13]. This difference in particle thickness along the FD and TD axis will be discussed in more detail in Section 3.2 of this paper.

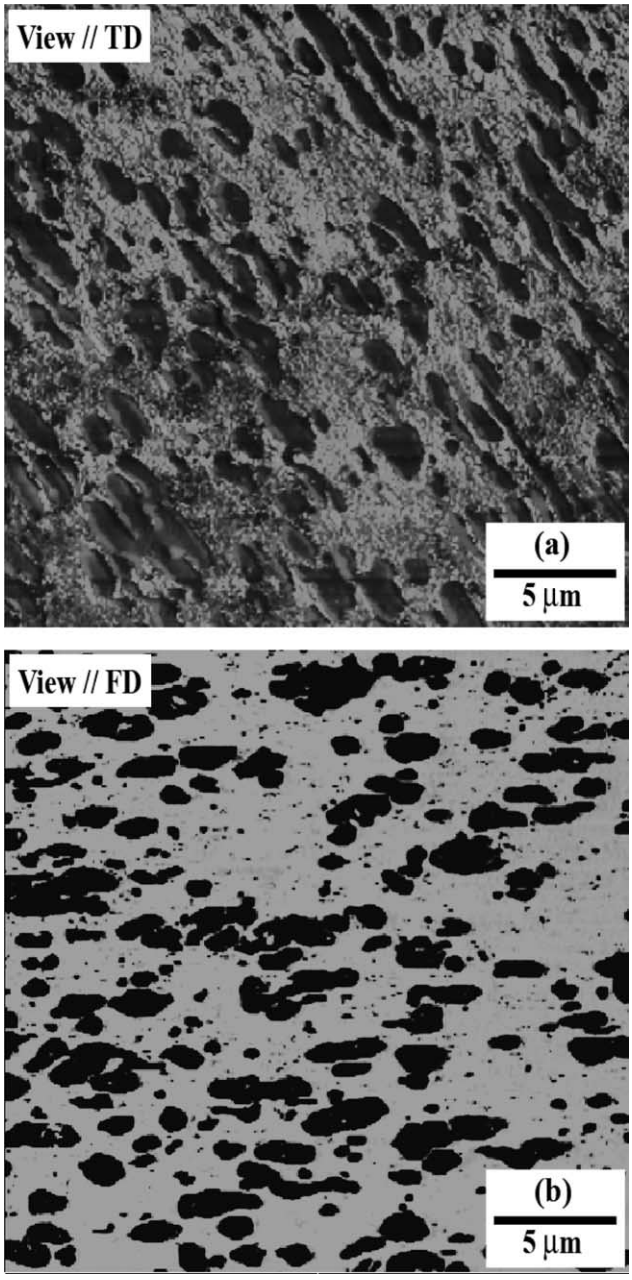


Fig. 3. AFM images of PP/elastomer/masterbatch nanocomposites to reveal rubber particle morphology. The materials contain 30 wt% elastomer and 2.8 wt% MMT. The images correspond to scans in the (a) FD–ND plane, (b) TD–ND plane. The samples were taken from the core of injection molded specimens.

Fig. 3 shows AFM images of PP/elastomer/masterbatch nanocomposites containing 30% elastomer and 2.8% MMT, which were viewed parallel to the TD and to the FD. In these nanocomposites, the elastomer particles are relatively well dispersed in the PP matrix with smaller size and more elongated shape than those in nanocomposites containing lower contents of MMT. At this composition, the particles seem to be more elongated along the FD (Fig. 3(a)) than the TD (Fig. 3(b)). The increased anisotropy in particle shape is further pronounced in nanocomposites with higher MMT contents, e.g. 6.8 wt% MMT. The effect of MMT content on the elastomer particle size and shape in these nanocomposites is discussed in this paper.

### *3.2. Particle analyses for PP/elastomer/masterbatch nanocomposites*

#### *3.2.1. Elastomer particle analysis*

As discussed in the previous paper [9], particle analysis for the elastomer phase in PP/elastomer/masterbatch nanocomposites is not a trivial task due to the fact that the particles are non-spherical with sizes and shapes that depend on MMT content. Fig. 4 shows the particle length (along the major axis), thickness (along the minor axis) and apparent particle diameter, $d$, that can be obtained by AFM image analysis in the two viewing planes, i.e. FD–ND and TD–ND planes, calculated from particle area as described in the figure. Views in the FD–TD plane were not made due to the experimental difficulties in preparing specimens for AFM experiments, particularly for nanocomposites containing higher elastomer concentrations. The number and weight average apparent particle diameters ($\bar{d}_{FD-ND}$,$\bar{d}_{TD-ND}$), lengths ($\bar{\ell}_{FD}$,$\bar{\ell}_{TD}$) and thicknesses ($\bar{t}_{ND,view||TD}$, $\bar{t}_{ND,view||FD}$) of the elastomer particles were calculated using the relationships described in the previous work [9]. A series of histograms of apparent particle diameter, length, and thickness along the FD and TD axes was built for the nanocomposites containing 30 wt% elastomer and various amounts of MMT. Fig. 5 shows typical distributions for elastomer particles viewed in the FD–ND plane for the nanocomposite containing 30 wt% elastomer and 6.8 wt% MMT. A summary of the elastomer particle size analyses, expressed as number and weight averages, obtained from views paralleled to the TD (FD–ND plane) and FD (TD–ND plane) for a series of nanocomposites containing 30 wt% elastomer with 0–6.8 wt% of MMT are shown in Table 1. The data obtained from the view in the TD–ND plane are taken from the previous paper [9], while those from the view in the FD–ND plane are reported here.

Fig. 6(a) shows the weight average apparent particle sizes as a function of MMT content, which were measured from AFM images viewed in the TD–ND plane ($\bar{d}_{TD-ND}$) and the FD–ND ($\bar{d}_{FD-ND}$). The average particle size as seen from either view decreases with addition of MMT, but the extent of reduction in ($\bar{d}_{FD-ND}$) is more apparent than in ($\bar{d}_{TD-ND}$). Data for ($\bar{d}_{FD-ND}$) for the blend without MMT could not obtained since the roughness of the microtomed surface made it difficult to resolve clear boundaries of large elastomer particles. However, it is expected that the particles as viewed in the FD–ND plane would be larger in size or longer in length than those viewed in the TD–ND plane due to the flow field during the injection molding process. Similar trends in average length (major axis) and thickness (minor axis) of elastomer particles as viewed in the two directions are also apparent, see Fig. 6(b). It is noticed that there are differences in the thickness of particles in the ND obtained for the two viewing planes; whereas, in principle, the values ought to be the same for ellipsoidal particles. This discrepancy may stem from the viewing plane not exactly matching the orthogonal coordinates and/or the complex shape of the elastomer particles induced by the 'barrier' effect of the clay particles as discussed in the previous paper [9]. These

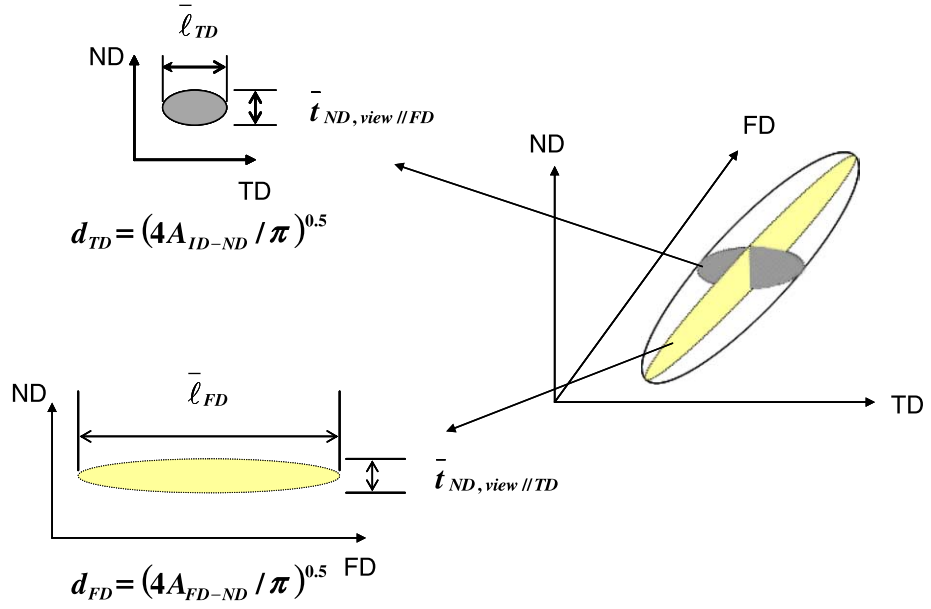


Fig. 4. Schematic illustration of elastomer particle length (major axis) and thickness (minor axis) obtained from AFM images plus definitions of average particle 'diameter' calculated from observed particle area.

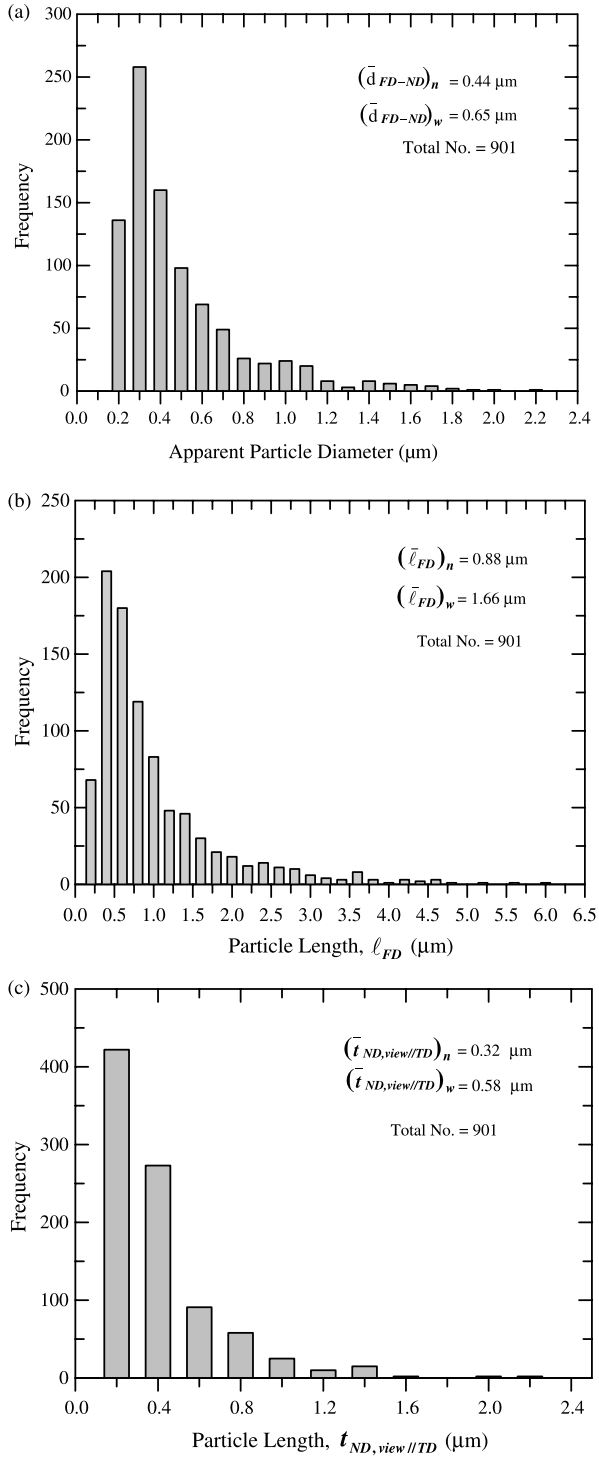


Fig. 5. Histograms of (a) apparent particle size computed from observed area, (b) length in the FD, and (c) thickness in the ND of elastomer particles obtained by analyzing AFM images of PP/elastomer/masterbatch nanocomposites containing 30 wt% elastomer and 6.8 wt% MMT. AFM images used for this analysis were taken from the core and viewed in the FD–ND plane.

complexities in shape of elastomer particles are quite pronounced for the nanocomposites containing higher MMT contents, as shown in AFM images of the previous paper.

Due to interfacial tension effects, the dispersed particles in a blend become more difficult to deform into elongated shapes as they become smaller. However, the elastomer particle aspect ratio, i.e. length/thickness, within a given viewing plane increases as the apparent particle size decreases for the current nanocomposites. Furthermore, the increase in the elastomer particle aspect ratio within the plane viewed parallel to the TD (FD–ND plane) is much more significant than that viewed parallel to the FD (TD–ND plane) as shown in Fig. 6(c). This may stem from the nature of the 'barrier' effect induced by the presence of the clay particles, which become oriented along the flow field generated by the injection molding process. It is important to note that the aspect ratio used here is the ratio of the weight average particle length to the weight average particle thickness, i.e. $(\bar{\ell})_w/(\bar{t})_w$; this ratio is not the same as the actual weight average aspect ratio of particles, i.e. $(\ell/t)_w$, which would be larger than $(\bar{\ell})_w/(\bar{t})_w$. These deformed elastomer particles within injection molded specimens seem to play an important role in the thermal expansion behavior of the current nanocomposites as will be discussed in more detail later.

Table 1
Elastomer particle size comparison for PP/elastomer/masterbatch nanocomposites containing 30% elastomer at different MMT contents

| MMT (wt%) | Plane of viewing | Length (major axis) (μm) | | Thickness (minor axis) (μm) | | $\bar{d}_n$ (μm) | $\bar{d}_w$ (μm) | Elastomer aspect ratio (length/thickness) | |
|---|---|---|---|---|---|---|---|---|---|
| | | $\bar{\lambda}_n$ | $\bar{\lambda}_w$ | $\bar{t}_n$ | $\bar{t}_w$ | | | $\bar{\lambda}_n/\bar{t}_n$ | $\bar{\lambda}_w/\bar{t}_w$ |
| 0 | TD–ND | 2.38 | 3.55 | 1.56 | 2.46 | 1.88 | 2.83 | 1.5 | 1.4 |
| 1 | TD–ND | 1.64 | 2.14 | 0.89 | 1.1 | 1.18 | 1.46 | 1.8 | 1.9 |
| | FD–ND | 1.89 | 2.54 | 1.33 | 1.78 | 1.52 | 1.99 | 1.4 | 1.4 |
| 2.8 | TD–ND | 1.08 | 1.94 | 0.52 | 0.77 | 0.69 | 1.03 | 2.1 | 2.5 |
| | FD–ND | 1.81 | 2.45 | 0.71 | 0.83 | 1.06 | 1.23 | 2.6 | 2.9 |
| 6.8 | TD–ND | 0.88 | 1.66 | 0.32 | 0.58 | 0.44 | 0.65 | 2.8 | 2.9 |
| | FD–ND | 1.04 | 1.52 | 0.25 | 0.35 | 0.45 | 0.51 | 4.2 | 4.3 |

### 3.2.2. Clay particle analysis

As shown in the previous paper [9] and in other literature [2,14,15], the aspect ratio of the filler has a significant effect on the properties of polymer-clay nanocomposites, which in turn is related to the degree of clay dispersion, e.g. exfoliated, agglomerated, or combinations of the two, as well as the inherent geometry of the pristine clay platelets. In our laboratory, a sizeable effort has been devoted to performing in-depth particle analysis using TEM photomicrographs to provide quantitative information regarding the relationship between clay structure and nanocomposites properties [15–18].

Fig. 7 shows typical histograms of MMT particle lengths, thickness, and their pertinent statistical data obtained on nanocomposites made from the PP/masterbatch containing 6.8 wt% MMT. The measurements were performed on particles observed in the TD–ND plane when viewed parallel to the FD. When these histograms are compared with those reported in the previous paper [9], which were obtained from the view parallel to the TD, noticeable differences in the trends of particle length, thickness and aspect ratio with varying MMT content are seen for nanocomposites formed from the PP/masterbatch. These differences are listed in Table 2 and shown in Fig. 8, in which the number and weight average

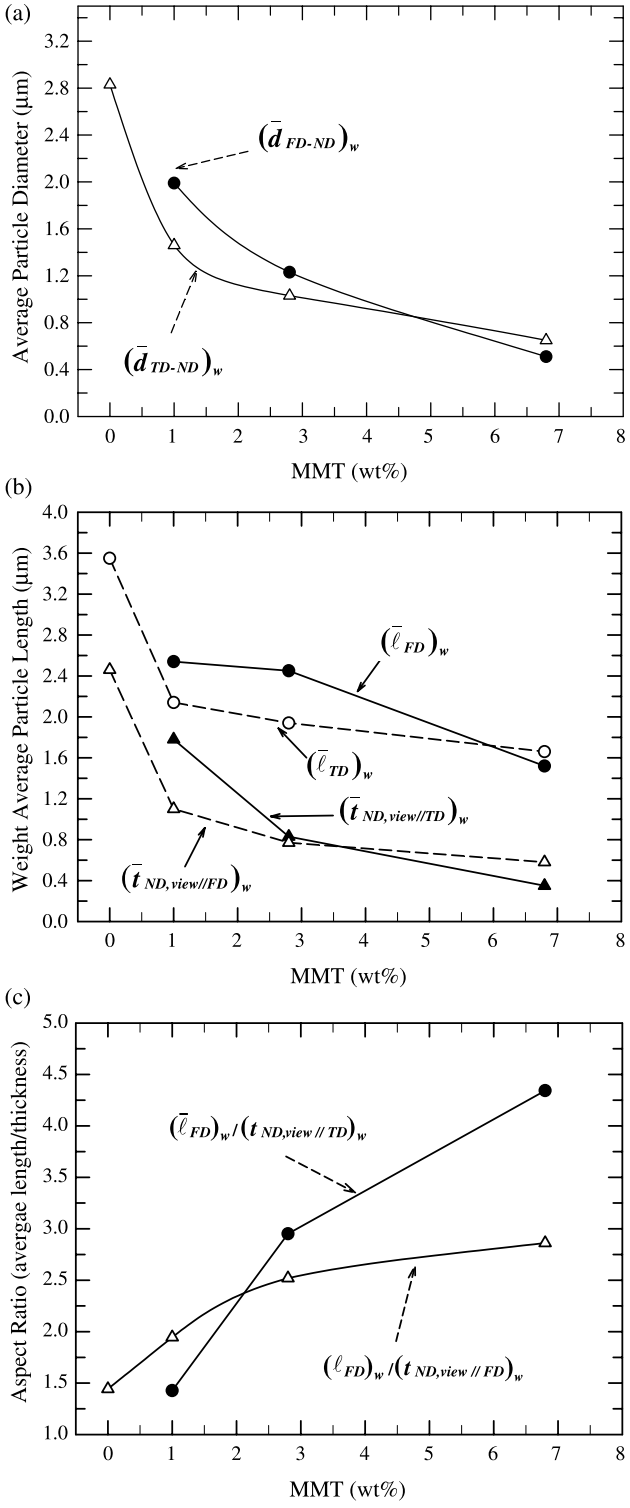


Fig. 6. The effect of MMT level on the (a) weight average apparent elastomer particle size, (b) weight average length and thickness and, (c) aspect ratio of elastomer particles as determined by scans normal to the FD and TD for PP/elastomer/masterbatch nanocomposites containing 30 wt% elastomer.

particle lengths, thicknesses, and aspect ratios of the clay particles along the FD and TD are compared based on results for the particle analysis in this and the previous paper. The average particle length along the TD, $\bar{\ell}_{TD}$, steadily decreases with increasing MMT concentration; whereas, the particle length along the FD, $\bar{\ell}_{FD}$, decreases sharply at low MMT contents and then does not change much with further addition of MMT as shown in Fig. 8(a). Interestingly, the trend of the average particle thickness with MMT content viewed along the TD is opposite to that along the FD; the average particle thickness viewed parallel to the FD decreases while the thickness viewed parallel to the TD increases as the MMT amount increases, Fig. 8(b). We propose the following explanation of these apparently contradictory trends.

The edges of the relatively large clay particles are somewhat splayed, i.e. peeled individual platelets and small stacks of platelets. The microtoming process for the views parallel to the FD (TD–ND plane) yields some sections from these edges while others come from the center of the particle, and the two look quite different. Fig. 9 shows schematically how the length and thickness of clay particles may appear differently in views parallel to the TD and FD and as the content of MMT increases. We propose that at low MMT contents, e.g. 1 wt% MMT, the shear stresses during melt processing are relatively low so

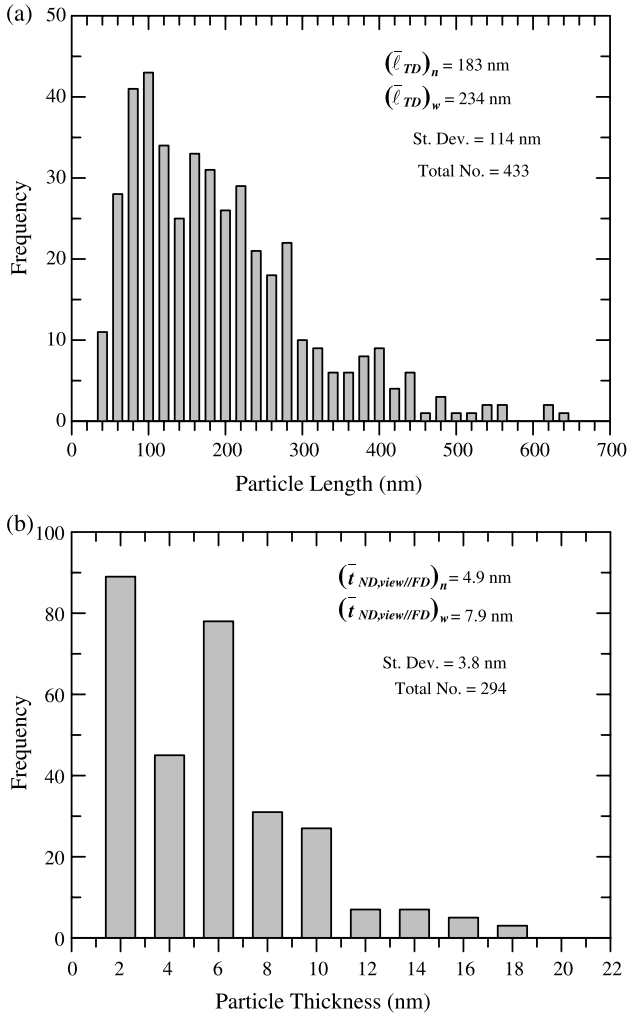


Fig. 7. Histograms of MMT particle (a) length and (b) thickness obtained by analyzing TEM micrographs of PP/masterbatch nanocomposites containing the 6.8 wt% MMT. Sections used for this analysis were taken from the core and were viewed parallel to the FD.

Table 2
Image analysis results for clay particles obtained from TEM micrographs of injection molded PP/masterbatch nanocomposites

| | Viewed parallel to TD | | | Viewed parallel to FD | | | |
|---|---|---|---|---|---|---|---|
| MMT concentration (wt%) | 1.0 | 2.8 | 6.8 | 1.0 | 2.8 | 4.8 | 6.8 |
| Number average particle length $\bar{\ell}_n$ (nm) | 288 | 221 | 225 | 271 | 230 | 202 | 183 |
| Weight average particle length $\bar{\ell}_w$ (nm) | 342 | 281 | 264 | 323 | 262 | 257 | 234 |
| Number average particle thickness $\bar{t}_n$ (nm) | 4.6 | 6.0 | 7.3 | 6.4 | 5.8 | 5.0 | 4.9 |
| Weight average particle thickness $\bar{t}_w$ (nm) | 6.1 | 8.6 | 10.5 | 8.9 | 8.8 | 7.2 | 7.9 |
| Particle aspect ratio, $\bar{\ell}_n/\bar{t}_n$ | 63 | 37 | 31 | 42 | 40 | 41 | 37 |
| Particle aspect ratio, $\bar{\ell}_w/\bar{t}_w$ | 56 | 33 | 25 | 36 | 30 | 36 | 30 |

that the clay particles are relatively large agglomerates with a long effective length. However, the shear stresses increase with clay loading because of the effect of melt viscosity. This increased shear force may cause more clay platelets to splay or peel apart with polymer penetrating the particles from the edges, as shown in Fig. 9. Intuitively, clay particles are expected to be better aligned along the FD than the TD due to the difference in stresses in these directions; indeed, this is observed for well-exfoliated nanocomposites like those based on nylon 6 [2]. However, in poorly exfoliated systems like these polyolefin nanocomposites, the clay particles still tend to align along the flow field, but the shear stress appears to cause the particles to bend and/or peel their edges apart, which may explain the large number of particles with skewed and/or tilted shape in views parallel to TD (FD–ND plane) as shown in Fig. 2(a), and may also explain the changes in clay particles when viewed parallel to the FD. Apparently, more splayed clay particle edges are seen in views parallel to the TD (FD–ND plane) than the FD (TD–ND plane) due to the higher shear stress along the flow direction. The proposed appearance of the clay particles in the view parallel to the FD shown in Fig. 9 is somewhat exaggerated in order to make clear our proposal about how the clay particles might appear in views parallel to FD using TEM. The average thickness of the clay particles observed decreases and more single platelets are seen with increasing MMT content as shown by the TEM particle analysis. Attrition of individual clay platelets and/or beak-up of larger clay agglomerates into small ones decrease the effective length of clay particles. The proposed evolution of clay particles with increasing MMT concentration, e.g. more peeled edges, more penetration of polymer into the edges of particles, and more break-up of larger particles, seem to explain the trends in particle length and thickness along the FD and TD shown in Fig. 8(a) and (b).

The apparent average aspect ratio of the clay particles along the FD decrease rapidly at lower contents of MMT and then decrease more gradually with further addition of MMT; whereas, the aspect ratio along the TD is nearly independent of the clay loading as shown Fig. 8(c). Again, the aspect ratio used here is the ratio of the average particle length to

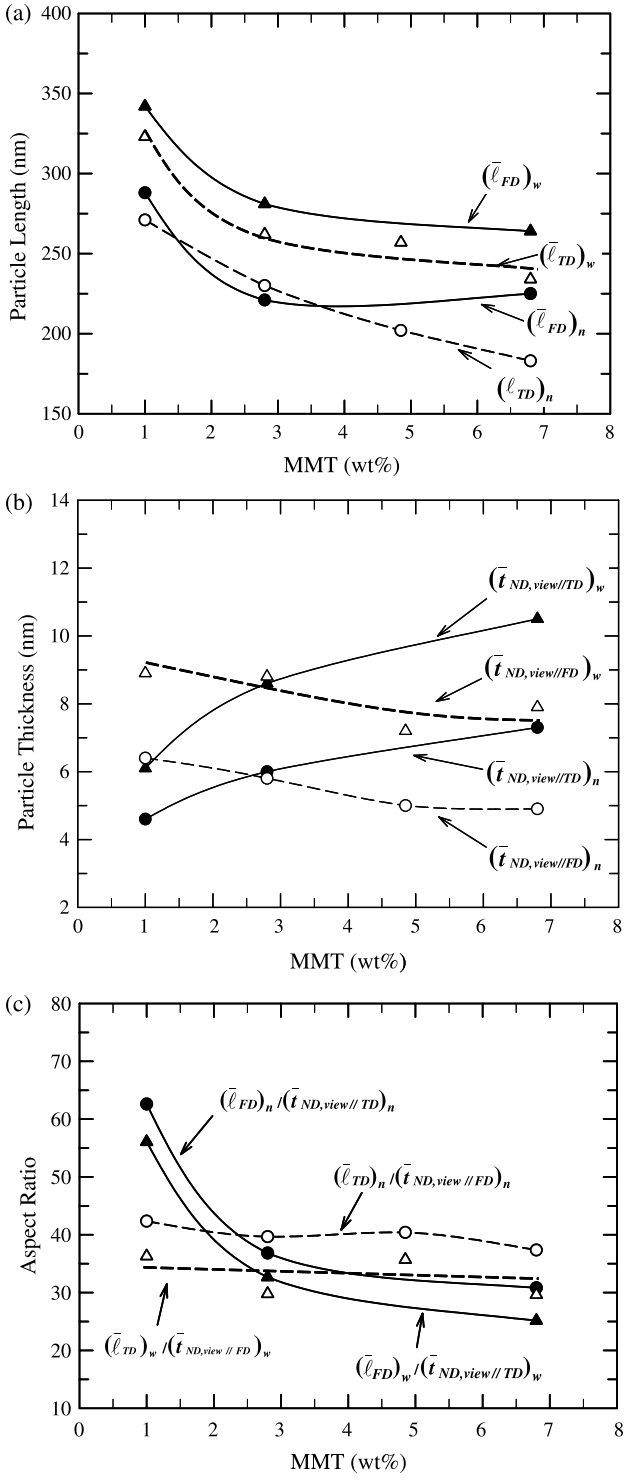


Fig. 8. The effect of MMT content on the (a) average lengths, (b) average thicknesses, and (c) aspect ratio of elastomer particles for PP/elastomer/masterbatch nanocomposites containing 30 wt% elastomer.

the average particle thickness, i.e. $(\bar{\ell})/(\bar{t})$, calculated from the values shown in Fig. 8(a) and (b), which is different from averaging the aspect ratios of individual particles, i.e. $\langle \ell/t \rangle$. The aspect ratio of clay particles along the TD at high MMT concentrations, $>3$–4 wt%, is somewhat higher than along the FD. This result seems to contradict the observed thermal

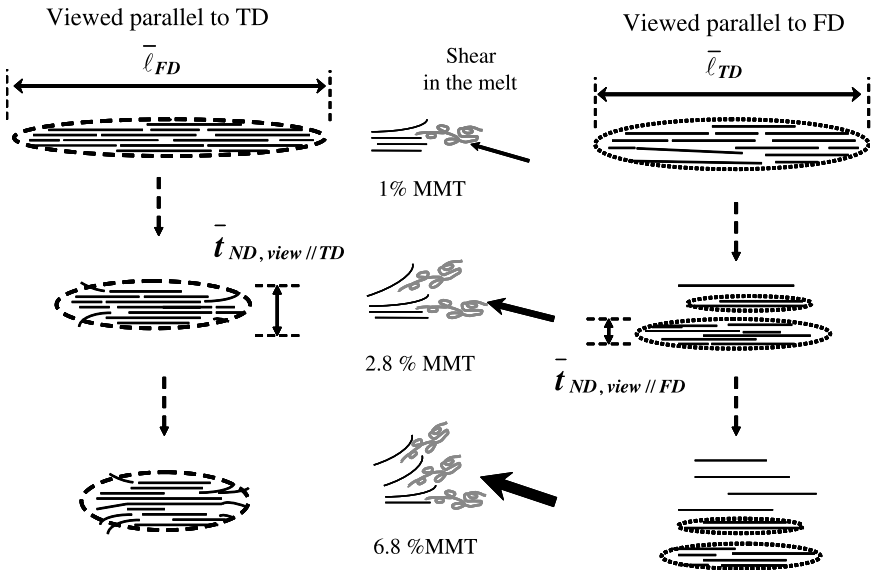


Fig. 9. Schematic illustration of the changes of effective MMT particle length and thickness when viewed along the FD and TD in PP/masterbatch nanocomposites as MMT content increases.

expansion behavior of PP/masterbatch nanocomposites (Section 3.3) since a higher aspect ratio of the filler should lead to a lower thermal expansion coefficient (CTE). As shown later, the reduction in CTE with MMT addition along the FD is much more significant than along the TD for PP/masterbatch nanocomposites; however, the aspect ratio values along the FD and TD seem to show an opposite trend, especially at higher MMT contents. This discrepancy can be explained by the fact that the average aspect ratio of clay particles in a view parallel to the FD (TD–ND plane) is largely calculated from the length and thickness of the peeled edges of the clay particles as described in Fig. 9. The thickness obtained from the view parallel to FD may not represent the actual thickness of the corresponding clay particles. So, the average aspect ratio value obtained from the view parallel to the FD may lead to an incorrect conclusion when used in composite theories to predict the thermal expansion behavior of the current nanocomposites. This issue will be discussed in more detail in the subsequent paper dealing with modeling of the properties of these nanocomposites.

### 3.3. Linear thermal expansion behavior of nanocomposites

Fig. 10 shows typical thermal expansion behavior of a PP/elastomer/masterbatch nanocomposite on the first and second heating. The specimen was heated to 125 °C during the first heating scan and then annealed for 30 min. As shown in Fig. 10, annealing at this elevated temperature eliminated the reduced thermal expansion observed above 60 °C during the first scan. This experimental protocol is similar to the thermal history experienced by automotive parts. Thus, the thermal expansion studies presented in this paper were performed using the above method. As shown in Fig. 10 and the literature, the PP and PP-based nanocomposites show significant non-linearity in thermal expansion as temperature increases. Thus, over the entire temperature range of interest, e.g. −30 to 100 °C, the CTE cannot be represented by a single value. There are a number of ways to deal with this issue, and one is to perform a linear regression of the digital thermal expansion data over any arbitrary number of temperature ranges. To pursue this approach, we selected the following ranges: −30 to 0, 0–30, 30–60, and 60–100 °C. Among these temperature ranges, the thermal expansion of the current nanocomposites in the temperature range of 0–30 °C is of particular interest since the thermal expansion data can be related to the mechanical property data measured at room temperature, i.e. ca. 25 °C. This issue will be discussed in more detail in the subsequent modeling paper. So, all data presented in this paper were obtained from 0 to 30 °C temperature range of the second heating scan of these nanocomposites.

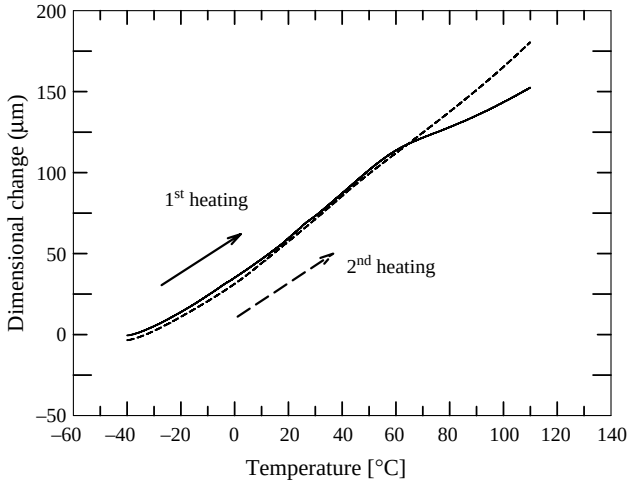


Fig. 10. Typical thermal expansion behavior of PP/elastomer/masterbatch nanocomposites in the FD during the first and second heating runs; in this example, the composition is 30 wt% elastomer and 2.8 wt% MMT.

Fig. 11 shows the measured linear thermal expansion coefficients, simply called CTE hereafter, in the flow and transverse directions over the 0–30 °C temperature range of the second heating as a function of MMT concentration for nanocomposites of different clay and elastomer contents. It is noted that the CTEs in the TD and ND (Fig. 11(b) and (c)) for the pure PP are slightly higher than that in the FD (Fig. 11(a)). This may be attributed to the polymer chain and/or crystallite orientation during the injection molding process. Polymer chains may be better oriented in the FD than in the TD or ND within the injection molded specimen, thus resulting in comparatively low CTE in the FD than in other directions. The orientation of polymer crystallites may have a similar effect on the CTE along different directions. Addition of elastomer to the PP leads to an increase in CTE in the FD, TD, and ND, as expected; however, the extent of the increase in the ND is significantly higher than that in the FD or in the TD, especially at high elastomer concentrations. Thermal expansion behavior of these nanocomposites is significantly altered by addition of MMT. CTE in the FD and TD is decreased as MMT content increases for all nanocomposites. The decrease in the flow direction is much more significant, especially as the amount of elastomer increases. Clearly, the thermal expansion of the current nanocomposites is affected by both the clay and elastomer phases. The addition of clay causes significant reductions in CTE in the TD at low loadings of clay, but the extent of reduction diminishes at higher MMT contents as shown in Fig. 11(b). Thermal expansion in the ND, Fig. 11(c), steadily increases as MMT content increases. For nanocomposites containing 40 wt% elastomer, the increase of thermal expansion in the ND is more significant than those containing lower content of MMT. Fig. 11(d) shows that the bulk expansion coefficient, obtained by adding the measured CTEs in the three directions, i.e. $\alpha_{bulk} = \alpha_{FD} + \alpha_{TD} + \alpha_{ND}$, is relatively unaffected by MMT content but increases with the amount of elastomer, as expected.

The CTE data in the flow and transverse directions shown above are re-plotted as a function of elastomer concentration in Fig. 12. The thermal expansion coefficient in the FD for compositions without clay steadily increases as the elastomer content increases as expected (Fig. 12(a)). The addition of MMT gradually alters the increase in CTE with increasing elastomer concentration. At high MMT content, the CTE initially increases, goes through a maximum, and eventually

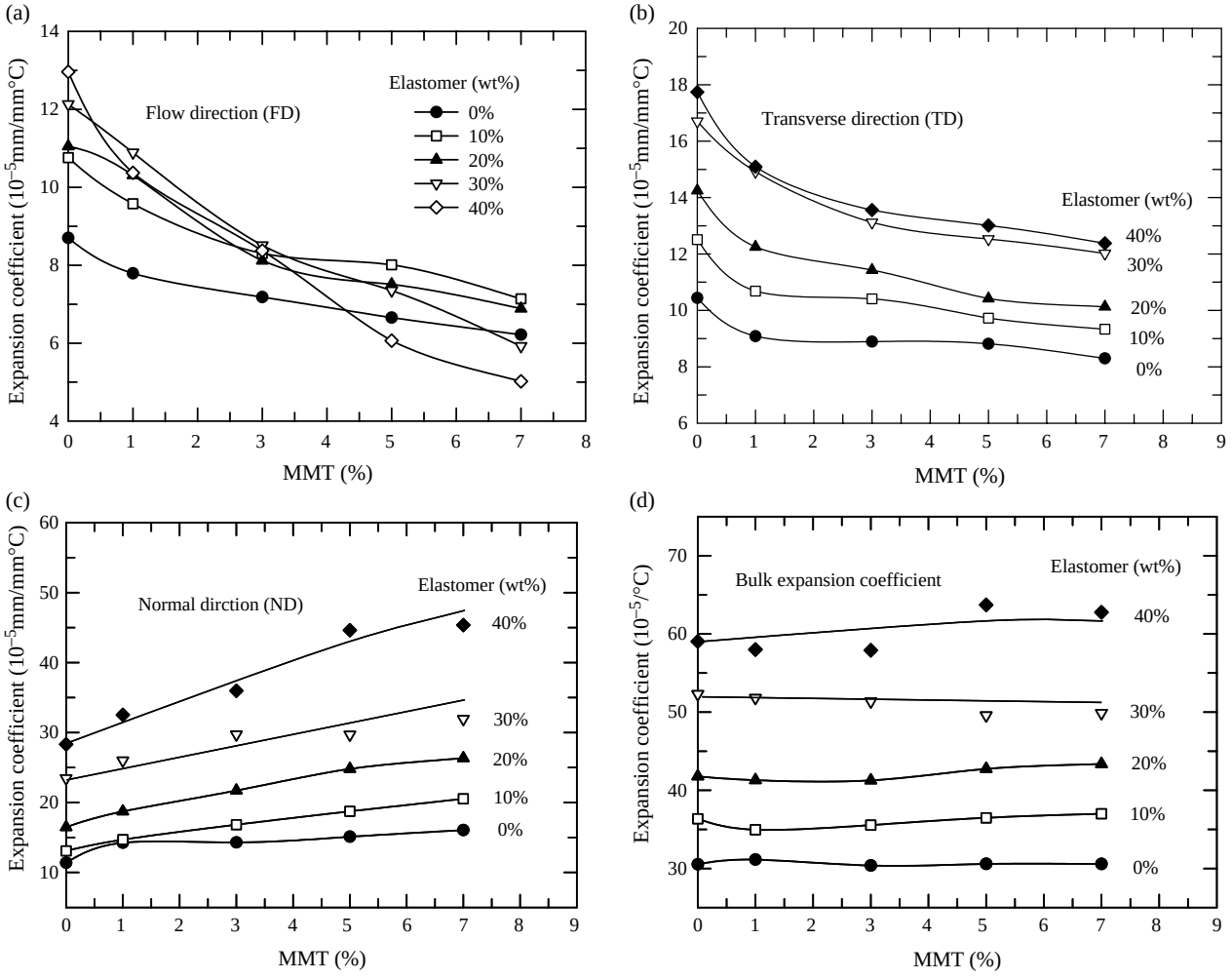


Fig. 11. Linear thermal expansion coefficients in the (a) FD, (b) TD, (c) ND, and (d) the bulk expansion coefficients for PP/elastomer/masterbatch nanocomposites as a function of MMT concentration.

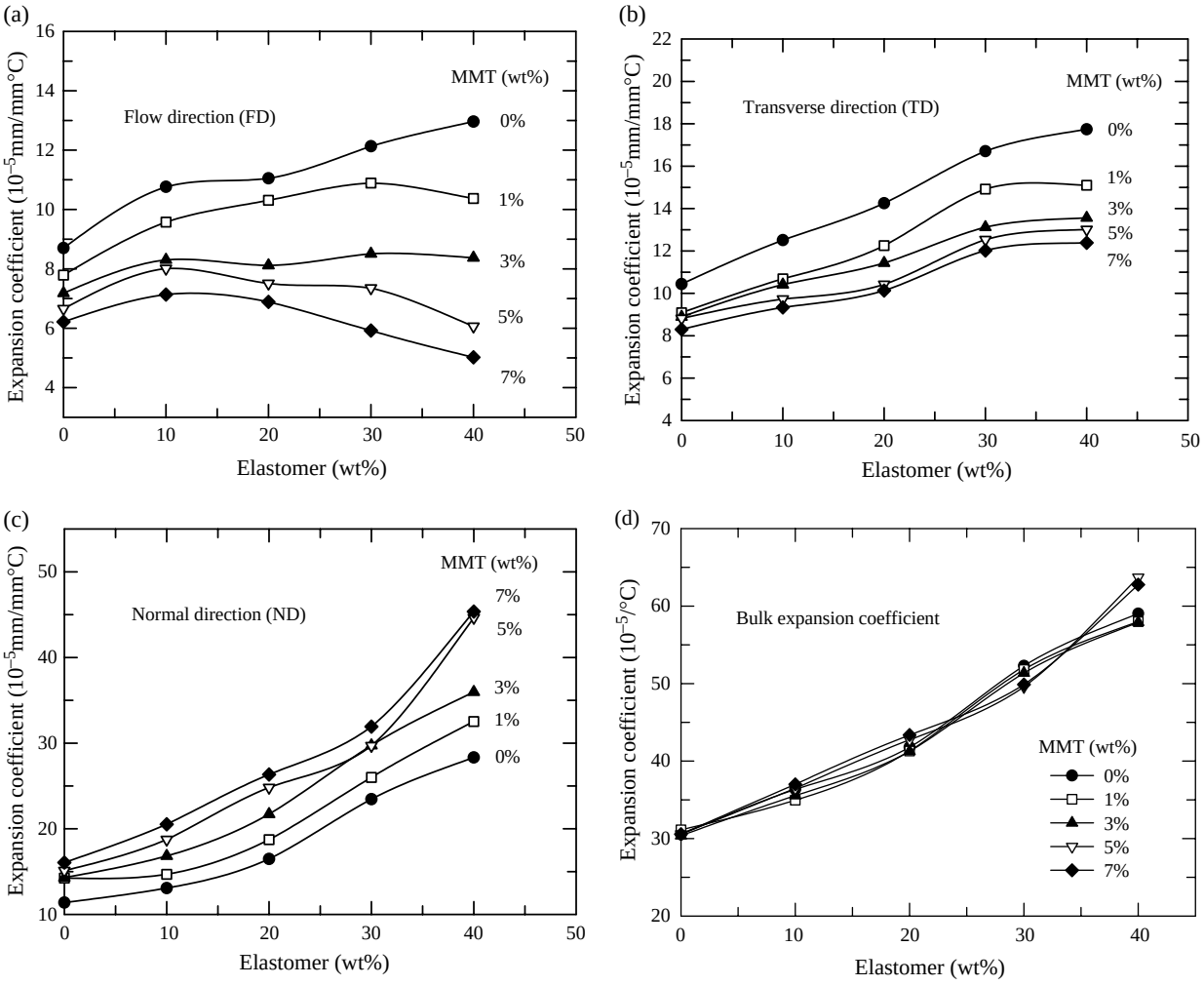


Fig. 12. Linear thermal expansion coefficients in the (a) FD, (b) TD, (c) ND, and (d) the bulk expansion coefficients for PP/elastomer/masterbatch nanocomposites as a function of elastomer concentration.

decreases as more elastomer is added. The CTE in the TD, Fig. 12(b), steadily increases with increasing elastomer content at all MMT levels with the same tendency for a decrease in slope between 30 and 40% elastomer. As shown in Fig. 12(c), the CTE in the ND strongly increases with increasing elastomer amount and appears to abruptly increase for compositions containing high elastomer and MMT contents. The bulk expansion coefficients shown in Fig. 12(d) increase with increasing elastomer concentration and are nearly independent of the MMT content. The trend of thermal expansion in the FD for the current nanocomposites looks counterintuitive. We must recall there are several factors that play roles in opposition to each other: (1) there is a morphological rearrangement in the ternary system, i.e. clay affects elastomer morphology, as described in this and the previous paper; (2) since the elastomer has a higher thermal expansion coefficient than PP or MMT, thermal expansion tends to increase as more elastomer is added, (3) adding the elastomer lowers the modulus and a lower modulus of the matrix makes it easier for MMT to restrain the expansion of the composite.

For better understanding of the relative change in the thermal expansion behavior of these nanocomposites, the CTE data in the FD shown in Fig. 12(a) are normalized first by the CTE of the corresponding PP/elastomer blend without MMT and plotted versus MMT content in Fig. 13(a) and then by the corresponding PP/masterbatch nanocomposite without elastomer and plotted versus elastomer content in Fig. 13(b). As seen in Fig. 13(a), the normalized CTE in the FD having a fixed elastomer content always decreases with increasing MMT content; however, the extent of reduction in CTE becomes greater as more elastomer is added. This may be explained by the greater mechanical constraint of the matrix by MMT when the modulus is lowered by addition of elastomer and to some extent changes in morphology.

Recently, a significant reduction in CTE was observed in polymer/rubber blends, e.g. PP/EPR, PA/EPR, etc. when the rubber domains were highly deformed into micro-layer or co-continuous structures, especially for blends containing high rubber concentrations, e.g. >40% [19]. The reduced CTE in the FD and TD for injection molded polymer blends was attributed to the higher expansion in the ND. The morphological changes of the rubber phase were achieved by controlling the rubber concentration and processing conditions. However, this is not the case for the current nanocomposites since the

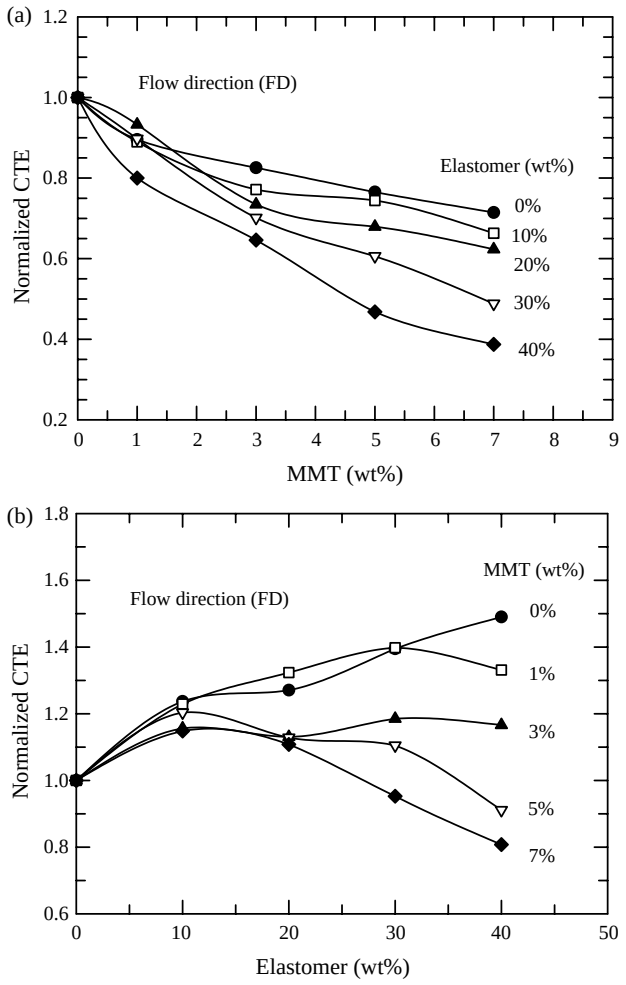


Fig. 13. Normalized linear thermal expansion coefficients in the flow direction for PP/elastomer/masterbatch nanocomposites as a function of (a) MMT and (b) elastomer concentration. Each plot uses the data from Fig. 12(a); in part (a) the values are divided by the CTE at the same elastomer content but without clay while in part (b) the values are divided by the CTE at the same MMT content but without elastomer.

CTE of PP/elastomer blends without clay continues to increase even at higher elastomer contents, e.g. 30 and 40% elastomer, as shown in Fig. 12(a). This discrepancy may stem from the different characteristics of the ethylene–octene elastomer used here and the ethylene–propylene elastomer used in their study and the relationships of these elastomers with the matrix, such as viscosity ratio, interfacial adhesion, etc. Such issues are beyond the scope of the current study; however, since addition of only elastomer to the PP without the filler results in the reduction of the mechanical modulus of the composites, it may not be useful for the applications where relatively high mechanical strength and low thermal expansion are required in any event.

The trends in thermal expansion behavior observed for the current nanocomposites seem to stem from greater mechanical constraint by the filler as the modulus of the polymer phase is reduced by addition of elastomer. The higher extent of the constraint and the resulting reduction in CTE is only achieved when the elastomer particles are well dispersed with highly elongated shapes in the nanocomposites containing higher elastomer and MMT contents. This point is clear in Fig. 13(b) where the FD thermal expansion coefficients of the nanocomposites (relative to the corresponding nanocomposite without elastomer) are plotted versus elastomer content. At low elastomer concentrations, e.g. 10 wt%, the normalized CTE increases with elastomer content for all nanocomposites. This may be due to the relatively large elastomer domains observed even at higher MMT concentrations; since large, spherical elastomer particles may limit the constraint effect caused by clay particles along the FD in spite of the reduction in modulus caused by addition of elastomer. Further addition of elastomer with no or low MMT contents results in a continued increase in CTE. At high MMT concentrations, the CTE decreases significantly as the amount of elastomer increases. This is due to the changes in the morphology of the elastomer phase, e.g. highly elongated in the FD with smaller particle sizes, in the nanocomposites containing higher elastomer concentrations of 30 and 40 wt%. This was shown in the morphology and particle analysis presented in this and previous papers. The combined effects from the reduction in the matrix modulus and the constraint effect by clay particles result in a greater reduction in CTE for nanocomposites with higher MMT and elastomer contents, e.g. 7% MMT and 40% elastomer. In addition, these morphological changes of the elastomer phase by addition of MMT have a considerable effect on other properties of the current nanocomposites such as Poisson's ratio.

## 4. Summary and conclusions

Significant reductions in linear thermal expansion coefficients were achieved by the addition of clay to PP/elastomer-based TPO nanocomposites prepared by melt processing. An in-depth analysis of the morphology by TEM and AFM of these nanocomposites and subsequent quantitative particle analyses for the dispersed clay and elastomer phases along the FD and TD in the injection molded specimens revealed that both clay and elastomer particles have anisotropic shapes, i.e. different effective length along the FD and TD directions. This anisotropy of the particles was further enhanced with increasing MMT and elastomer content. Additionally, particle analyses revealed that the dimensions of both clay and elastomer particles are highly dependent on the MMT concentration in the nanocomposite. The average thickness of clay particles viewed parallel to the FD decreased with increasing MMT content; whereas, the thickness of the clay particles viewed parallel to the TD increased as MMT content increased. These differences in apparent morphology according to direction of viewing is, we believe, an artifact, which mainly stems from the increased amount of peeled edges of clay particles that can be seen in the views parallel to the FD of TEM photomicrographs as MMT content increased. On the other hand, the addition of more than 1 wt% MMT resulted in a greater increase in aspect ratio of elastomer particles along the FD. The extent of the increase along the TD is much less compared to that along the FD. This anisotropy of elastomer

particles is largely due to the higher melt viscosity and 'barrier' effect of clay particles as discussed in the previous paper.

Thermal expansion in the FD and TD decreased as MMT content increased for all nanocomposites, but the decrease in the flow direction was much more significant, especially as the amount of elastomer increased. On the other hand, thermal expansion in the ND steadily increased as MMT content increased. The bulk expansion coefficient was relatively unaffected by MMT content but increased with the amount of elastomer. These trends in thermal expansion of the current nanocomposites with varying MMT and elastomer amounts were explained in terms of analyses of the clay and elastomer particle dimensions. The morphology attained and the resulting mechanical and thermal properties of the current nanocomposites are far from the ultimate ones that can be predicted based on composite theory. The latter indicates that further efforts to reach complete exfoliation of the clay and might lead to even better properties of such nanocomposites.

## Acknowledgements

The authors thank General Motors for funding this work and the permission to publish it. The authors would like to thank Dr. Douglas Hunter of Southern Clay Products for technical assistance and for providing materials.

## References

[1] Segal L. Polym Eng Sci 1979;19(5):365–72.
[2] Yoon PJ, Fornes TD, Paul DR. Polymer 2002;43(25):6727–41.
[3] Holliday L, Robinson J. J Mater Sci 1973;8:301–11.
[4] Chow TS. J Polym Sci, Polym Phys Ed 1978;16(6):967–70.
[5] Okada A, Usuki A. Mater Sci Eng 1995;C3:109–15.
[6] Yui H, editor. Design of plastic composite materials. 3rd ed. Tokyo: Plastics Age; 1992.
[7] Fasulo PD, Rodgers WR, Ottaviani RA, Hunter DL. Polym Eng Sci 2004; 44(6):1036–45.
[8] Materials provided by Hunter DL of Southern Clay Products Inc.
[9] Lee HS, Fasulo PD, Rodgers WR, Paul DR. Polymer 2005;46: 11673–89.
[10] Yalcin B, Cakmak M. Polymer 2004;45(19):6623–38.
[11] Park H-M, Liang X, Mohanty AK, Misra M, Drzal LT. Macromolecules 2004;37(24):9076–82.
[12] Fornes TD, Yoon PJ, Keskkula H, Paul DR. Polymer 2001;42(25): 9929–40.
[13] Ton-That MT, Perrin-Sarazin F, Cole KC, Bureau MN, Denault J. Polym Eng Sci 2004;44(7):1212–9.
[14] Vaia RA, Giannelis EP. MRS Bull 2001;26(5):394–401.
[15] Fornes TD, Paul DR. Polymer 2003;44(17):4993–5013.
[16] Chavarria F, Paul DR. Polymer 2004;45(25):8501–15.
[17] Fornes TD, Hunter DL, Paul DR. Macromolecules 2004;37(5): 1793–8.
[18] Fornes TD, Hunter DL, Paul DR. Polymer 2004;45(7):2321–31.
[19] Wu G, Nishida K, Takagi K, Sano H, Yui H. Polymer 2004;45(9): 3085–90.